

June, 1994

CMU-HEP94-20  
DOE/ER/40682-74  
PITT-94-06  
hep-ph/9406422

# Thermal Activation Rates in the Chirally Asymmetric Gross-Neveu Model

Daniel Boyanovsky<sup>1(a)</sup>, David E. Brahm<sup>2(b)</sup>,  
Richard Holman<sup>3(b)</sup>, and Da-Shin Lee<sup>4(a)</sup>

<sup>(a)</sup>*Dept. of Physics and Astronomy, University of Pittsburgh, Pittsburgh PA 15260*

<sup>(b)</sup>*Carnegie Mellon Physics Dept., Pittsburgh PA 15213*

## Abstract

We address the problem of how to incorporate quantum effects into the calculation of finite-temperature decay rates for a metastable state of a quantum field theory. To do this, we consider the Gross-Neveu model with an explicit chiral symmetry breaking term, which allows for a metastable state. This theory can be shown to have a “critical bubble” which is a solution to the *exact* equations of motions (*i.e.* to all orders in perturbation theory, including all higher derivative, quantum and thermal corrections). This configuration mediates the thermal activation of the metastable vacuum to the true ground state, with a decay rate  $\Gamma \propto \exp(-F_c/T)$ , where  $F_c$  is the free energy of the critical bubble. We then compare this exact calculation to various approximations that have been used in previous work. We find that these approximations all *overestimate* the activation rate. Furthermore, we study the effect of finite baryon number upon the bubble profile and the activation barriers. We find that beyond a critical baryon number the activation barriers disappear altogether.

---

<sup>1</sup>Email: boyan@vms.cis.pitt.edu

<sup>2</sup>Email: brahm@fermi.phys.cmu.edu

<sup>3</sup>Email: holman@cmphys.phys.cmu.edu

<sup>4</sup>Email: dashin@phyast.pitt.edu

# 1 Introduction and Motivation

Thermally activated reactions appear in many contexts, including chemical reactions[1], cosmological phase transitions[2], and sphaleron-mediated baryon number violating transitions in the early universe[3]. The physically important quantity in these transitions is the activation rate; this sets the time scale for the process, and determines whether these reactions can be in local thermal equilibrium.

There is a standard way of computing the activation rate in a field theory at finite temperature. Consider a field theory with a metastable false vacuum state as well as a stable ground state. The first step in the calculation is to construct a static, extremal configuration, corresponding to a critical bubble, in which the field is near the true vacuum on the inside, and in the false vacuum outside the bubble. Once this configuration is obtained, the activation rate  $\Gamma$  is proportional to  $\exp(-F_c/T)$ , where  $T$  is the temperature, and  $F_c$  is the free energy of the critical bubble.

In most applications, the bubble configuration used in practice is a static extremum of the *classical* action[4, 5]. However, this leaves open the question of how to incorporate quantum effects into the rate calculation[6]. In particular, it is not clear whether the *full* theory has a critical bubble. Even if it does, the relation between the rate obtained by the using the classical bubble and the rate we would calculate using the exact bubble is not altogether clear, to say the least.

In a general field theory, it is usually impossible to construct the exact critical bubble of the theory, so that the questions asked above are moot. Nonetheless, it would be of great interest to have some idea of how the exact and the approximate rates compare. It is for this reason that we consider the Gross-Neveu[7] (GN) model in  $1 + 1$  dimensions. In the presence of a chiral symmetry breaking term, the theory has a metastable ground state. Of greater use to us, however, is the fact that we can obtain the *exact* critical bubble of the full quantum theory! Being able to do this allows us to proceed with the program described above. In particular, there are *no* “missing loops”, or higher derivative corrections. While this is a theory in  $1 + 1$  dimensions, the fact that it has much of the same richness as  $3 + 1$  theories (*e.g.* asymptotic freedom, dimensional transmutation, etc.) leads us to think that some of the results of this paper could be applicable to realistic field theories with metastable vacua in  $3 + 1$  dimensions.

In the next section, we describe the Gross-Neveu model in detail. In particular, we exhibit the phase structure of the theory in the presence of an explicit chiral symmetry breaking term, and construct the exact bubble for this theory. We then proceed to compare the exponential part of the activation rate obtained from the exact bubble to that found from various commonly used approximations, such as the Landau-Ginzburg approximation, amongst others. We next calculate the activation rate in the presence of finite fermion

number. Here we find that beyond a critical baryon number, the activation barriers disappear completely. Finally, section 5 contains our conclusions.

## 2 The N-flavor Gross-Neveu Model

We consider the Lagrangian density for the N-flavor Gross-Neveu[7] model in  $(1+1)$  dimensions:

$$\mathcal{L} = \bar{\psi}_\alpha(i\partial\!\!\!/ + m_0)\psi_\alpha + \frac{\lambda_0}{2N}(\bar{\psi}_\alpha\psi_\alpha)^2 \quad (1)$$

with  $\alpha = 1 \cdots N$  and a summation convention on  $\alpha$  is used. Introducing an auxiliary (Hubbard-Stratonovich) scalar field  $\Delta_0$ , the Lagrangian density becomes

$$\mathcal{L} = \frac{-\Delta_0^2 N}{2\lambda_0} + \bar{\psi}_\alpha(i\partial\!\!\!/ + m_0 + \Delta_0)\psi_\alpha \quad (2)$$

For  $m_0 = 0$  the Gross-Neveu model has a *discrete* chiral symmetry:

$$\psi_\alpha \rightarrow i\gamma_5\psi_\alpha \ ; \ \bar{\psi}_\alpha \rightarrow \bar{\psi}_\alpha i\gamma_5 \ ; \ \Delta_0 \rightarrow -\Delta_0$$

It is this symmetry that will be spontaneously broken (only discrete symmetries can be spontaneously broken in  $1+1$  dimensions). The explicit mass term  $m_0$  introduces an explicit chiral symmetry breaking term and will be responsible for a non-degenerate vacuum structure.

We should note that at tree level, the field  $\Delta$  has *no* dynamics; it is truly an auxiliary field. However, it acquires dynamical content by dint of quantum effects arising from integrating out the fermions[8].

### 2.1 The Gap Equation

Let us first consider homogeneous configurations  $\Delta(x) = \Delta$  and the case of zero temperature. In order to understand this case clearly, it is convenient to pass to the Hamiltonian

$$H = \int dx \left\{ \frac{\Delta_0^2 N}{2\lambda_0} + \psi_\alpha^\dagger \left[ -i\sigma_3 \frac{d}{dx} + \sigma_1 M_0 \right] \psi_\alpha \right\} \quad (3)$$

with  $M_0 = m_0 + \Delta_0$  being the effective fermion mass, and the  $\sigma_i$  are the Pauli matrices. The ground state is obtained by filling up the negative energy Dirac sea, so that the ground state energy density is given by:

$$\frac{E}{NL} = \frac{\Delta_0^2}{2\lambda_0} - \frac{1}{\pi} \int_0^\Lambda dk \sqrt{k^2 + M_0^2} \quad (4)$$

where  $L$  is the spatial length of the system and  $\Lambda$  an upper momentum cutoff. Dropping a term proportional to  $\Lambda^2$  (normal ordering) the energy density becomes

$$\frac{E}{NL} = \frac{\Delta_0^2}{2\lambda_0} - \frac{M_0^2}{4\pi} - \frac{M_0^2}{2\pi} \ln \left( \frac{2\Lambda}{|M_0|} \right) \quad (5)$$

while the gap equation ( $\partial E / \partial \Delta_0 = 0$ ) becomes

$$\frac{\Delta_0}{\lambda_0} = \frac{M_0}{\pi} \ln \left( \frac{2\Lambda}{|M_0|} \right) \quad (6)$$

Clearly both the energy density and the gap equation need non-trivial renormalizations. We find that the proper renormalization conditions are

$$M_0 = M_R = \Delta_R + m_R \quad (7)$$

$$\frac{1}{\lambda_R} = \frac{1}{\lambda_0} - \frac{1}{\pi} \ln \left( \frac{2\Lambda}{\kappa} \right) \quad (8)$$

$$\frac{M_R}{\lambda_0} - \frac{m_0}{\lambda_0} = \frac{M_R}{\pi} \ln \left( \frac{2\Lambda}{|M_R|} \right) \quad (9)$$

$$\frac{m_0}{\lambda_0} = \frac{m_R}{\lambda_R} \quad (10)$$

where  $\kappa$  is an arbitrary renormalization scale. The renormalized gap equation now becomes:

$$\frac{M_R}{\lambda_R} - \frac{m_R}{\lambda_R} = \frac{M_R}{\pi} \ln \left( \frac{\kappa}{|M_R|} \right) \quad (11)$$

We see that for  $m_R = 0$  the gap equation generates dynamically a scale

$$|\Delta_g| = \kappa e^{-\pi/\lambda_R} \quad (12)$$

This solution to the gap equation has the lowest energy (see below), thus spontaneously breaking the discrete chiral symmetry. It is convenient to absorb this dynamically generated scale as the overall scale in the problem and define all dimensionful quantities in terms of this scale. We thus introduce the following *dimensionless* quantities

$$M = \frac{M_R}{|\Delta_g|} ; \quad m = \frac{m_R}{|\Delta_g|} \quad (13)$$

Discarding terms independent of  $M$ , the *dimensionless* energy density becomes

$$\frac{E}{NL|\Delta_g|^2} = \frac{M^2}{4\pi} [\ln(M^2) - 1] - \frac{Mm}{\lambda_R} \quad (14)$$

and the gap equation becomes

$$\frac{M}{2\pi} \ln(M^2) = \frac{m}{\lambda_R}. \quad (15)$$

Clearly, for  $m = 0$  the solution  $M = \pm 1$  gives the lowest energy, thus the discrete chiral symmetry is indeed spontaneously broken.

The above energy density for a *constant*  $\Delta_R$  configuration is identified as the fully renormalized effective potential for the auxiliary scalar field.

At finite temperature  $\bar{T}$  we compute the free energy for the constant configuration and thus obtain the finite temperature effective potential. The free energy is given by

$$F[\Delta] = -\bar{T} \ln(\text{Tr} \exp(-H[\Delta]/\bar{T})) \quad (16)$$

where the trace is over the fermionic degrees of freedom. Discarding irrelevant terms, and introducing (along with  $M$ ,  $m$  above) the dimensionless temperature  $T = \bar{T}/|\Delta_g|$ , we find the dimensionless free energy per unit length to be (see Fig. 1)

$$V_{\text{eff}}(M) \equiv \frac{F[M]}{NL|\Delta_g|^2} = \frac{M^2}{4\pi} [\ln(M^2) - 1] - \frac{Mm}{\lambda_R} - \frac{2T^2}{\pi} I\left(\frac{M}{T}\right) \quad (17)$$

$$I(y) \equiv \int_0^\infty dx \ln \left[ 1 + e^{-\sqrt{x^2+y^2}} \right] \quad (18)$$

A small- $y$  expansion of  $I(y)$  is given by[9]

$$I(y) = \frac{\pi^2}{12} + \frac{y^2}{4} [\ln(y/\pi) + \gamma - 1/2] - \frac{7\zeta(3)}{64\pi^2} y^4 + \mathcal{O}(y^6) \quad (19)$$

where  $\gamma \approx 0.5772$  is Euler's constant and  $\zeta(3) \approx 1.202$  is the Riemann zeta function.

The extrema of the free energy are obtained from the gap equation:

$$\frac{M \ln M^2}{2\pi} - \frac{2T}{\pi} I'\left(\frac{M}{T}\right) = \frac{m}{\lambda_R} \quad (20)$$

This equation can either have three solutions (corresponding to a local minimum [metastable state] at  $M = M_- < 0$ , a maximum, and a global minimum [stable state] at  $M = M_+ > 0$  of the free energy), or just one solution (minimum). The left hand side of (20) that determines the local minimum at  $M_-$  is plotted in Fig. 2 for various values of  $T$ ; we see that solutions only exist for  $m/\lambda_R \leq 1/(e\pi) \approx 0.117$ , and for a given  $m$  only over a certain range of  $T$ 's (*e.g.* for  $m = 0$ ,  $T \leq e^\gamma/\pi \approx 0.567$ ).

## 2.2 The “Bubble” Configuration

Static topological and non-topological semiclassical solutions in the Gross-Neveu model have been analyzed and systematically constructed by Dashen, Hasslacher and Neveu (DHN)[10] and Campbell and Liao[11] using inverse scattering techniques. These solutions were also studied within the context of electron-phonon models of conjugate polymers[12, 13, 14, 15] and we refer the reader to these references for a comprehensive analysis of these solutions.

For the case  $m = 0$  (explicit chiral symmetry) there are two degenerate solutions to the gap equation. In this case there exist semiclassical topological soliton (kink) solutions and non-topological bubble (polaron) solutions[10, 11, 12]. However when  $m \neq 0$ , the effective potential (or free energy density) has one local and one global minimum, the degeneracy is lifted by the explicit chiral symmetry breaking mass term and no soliton solutions are available. However, by taking the results from the degenerate case, it is straightforward to find that in the  $m \neq 0$  case there still exist bubble solutions for which the “gap” parameter  $\Delta$  (and therefore  $M$ ) is spatially varying. These solutions (obtained via inverse scattering methods[10, 11, 12]) are given by

$$M_{\pm}(x) = M_{\pm} - k_0 \{ \tanh[k_0(x - x_0 + y)] - \tanh[k_0(x - x_0 - y)] \} \quad (21)$$

where  $M_{\pm}$  are the minima solutions to the gap equation (20). The parameters  $k_0$  and  $y$  are related by the “integrability condition”[10, 11, 12]

$$\tanh[2k_0 y] = \frac{k_0}{M_{\pm}}. \quad (22)$$

Note that we may take  $k_0 \geq 0$  since the sign of  $k_0$  cancels on both sides of the equation. Furthermore, notice that the solution requires that  $|y| \geq 1/|2M_{\pm}|$ . This is because the bound states cannot be localized in distances smaller than the Compton wavelength of the fermion. The position of the center of mass of the bubble is determined by  $x_0$ . This variable reflects the underlying translational invariance of the system. Because of this invariance, the energy (or free energy) is independent of this variable. For notational simplicity we will take it to be zero in the rest of the analysis.

The fermion spectrum in presence of this non-topological semiclassical configuration is also known exactly[11, 12, 13, 14, 15]:  $N$  bound states at energies

$$\pm w_{0\pm} = \pm \sqrt{M_{\pm}^2 - k_0^2}, \quad (23)$$

and positive and negative energy continuum states with energies  $\pm w_{k\pm} = \pm \sqrt{M_{\pm}^2 + k^2}$  and phase-shifts

$$\delta(k) = 2 \tan^{-1} \left( \frac{k_0}{k} \right). \quad (24)$$

with  $k_0$  the solution of the integrability equation (22). The exact fermionic wave-functions may be found in reference[12]. A noteworthy feature of these wave-functions is that the bound-state fermionic wave-functions are localized at  $x = \pm y$ . It is known[16, 17] that in the presence of a topological soliton (kink) there are fermionic zero modes whose wave-functions are localized at the position of the kink. Since the bubble configuration is reminiscent of a kink-antikink pair separated by a distance  $\approx 2|y|$ , the localized fermion bound-states are

the symmetric and antisymmetric combination of the zero-mode wave-functions, split off in energy because of the non-zero overlap of these wave-functions.

The above configuration, being similar to a kink-antikink pair separated by a distance  $2|y|$ , can clearly be identified with a “bubble”. The value of  $y$  (the remaining unspecified parameter) may be obtained by extremizing the energy of this configuration as a function of this parameter. For the moment we will leave this parameter free and treat it as a “collective coordinate”.

Before proceeding to the numerical analysis of the bubble energy, it proves illuminating to understand some features of this configuration.

Asymptotically this solution reaches  $M_{\pm}$ . For the global minimum  $M_+ > 0$  and the integrability condition (22) implies that  $y > 0$ . In this case, in the region  $-y < x < y$ , the bubble samples a region where the free energy (or energy) density is *higher* than that of the global minimum (for large  $y$ , probing the metastable state). Thus, for large  $y$ , the energy as a function of  $y$  will *grow* linearly (because the difference of the tanh’s is roughly constant in this region). On the other hand, if the bubble solution has its asymptotics in the *metastable* minimum for which  $M_- < 0$ , then  $y < 0$  and the bubble configuration is probing a region ( $y < x < -y$ ) in which the free energy (or energy) density is *lower*, thus *gaining* volume energy. In this case for large  $y$  the energy of the bubble configuration will *diminish* (linearly for large  $|y|$ ). Certainly for small  $y$  the spatial variations of the bubble configuration will raise the energy, and since for large  $y$  the energy will diminish, there has to be a maximum of the energy as a function of  $y$ . This maximum, the critical bubble, thus corresponds to a “sphaleron” in the sense of Manton and Samols[18]. The maximum of the energy as a function of the collective coordinate  $y$  corresponds to a saddle point in functional space. The unstable coordinate corresponds to  $\delta y = y - y^*$  where  $y^*$  corresponds to the maximum of the energy. The collective coordinate  $x_0$  corresponding to the center of mass of the bubble is a flat direction in functional space, along which the energy is constant as a consequence of translational invariance. This configuration is an *exact saddle point* of the full effective action (functional of  $\Delta(x)$ ) obtained after integrating out the fermions

$$S_{eff} = N \int d^2x \left\{ -\frac{\Delta_0^2}{2\lambda_0} \right\} - iN \text{Tr} \ln[i\cancel{\partial} + m_0 + \Delta_0]. \quad (25)$$

Finite temperature enters in the trace via the boundary conditions on the fermionic fields. In references ([10, 11, 12]) the effective action is written in terms of the scattering data (bound state energies and normalization and phase shifts) and the bag configuration is found by extremizing the full effective action with respect to these parameters. (This is the essence of the inverse scattering method). In the large  $N$  limit the functional integral is determined completely by the saddle points. However, even for finite  $N$ , the critical droplet configuration is an *exact* saddle point of the effective action.

Hereafter we will choose (making use of dimensional transmutation) the renormalization scale  $\kappa$  to be the value (analogous to  $\Lambda_{\text{QCD}}$ ) for which  $\lambda_R = 1$ . In units of the dynamically generated scale, the renormalized free energy difference between the metastable bubble configuration and that of the constant “gap” configuration in the metastable state is

$$\begin{aligned} \frac{F}{N} &= \frac{1}{2} \int dx \left( \Delta^2(x) - \Delta_-^2 \right) - w_{0-} - \int_0^{\kappa/2} \frac{dk}{\pi} \frac{d\delta}{dk} w_{k-} + \frac{2k_0}{\pi} \\ &- 2T \ln \left[ 1 + e^{-w_{0-}/T} \right] - 2T \int_0^\infty \frac{dk}{\pi} \frac{d\delta}{dk} \ln \left[ 1 + e^{-w_{k-}/T} \right] \end{aligned} \quad (26)$$

The phase-shift  $\delta(k)$  is given by (24), the bound state energy  $w_{0-}$  is given by (23), and  $w_{k-}$  are the continuum energies.  $F/N$  then simplifies to

$$\begin{aligned} \frac{F}{N} &= \frac{k_0}{\pi} \left[ 4\pi m y + 2 - \ln M_-^2 - \frac{2w_{0-}}{k_0} \tan^{-1} \left( \frac{k_0}{w_{0-}} \right) \right] \\ &- 2T \ln \left( 1 + e^{-w_{0-}/T} \right) + \frac{4Tk_0}{\pi} \int_0^\infty \frac{dk}{k^2 + k_0^2} \ln \left( 1 + e^{-w_{k-}/T} \right) \end{aligned} \quad (27)$$

The first term inside the square brackets shows that the energy diminishes for large  $|y|$  (recall  $y < 0$ ), consistent with the argument presented above. This is the classical “volume” energy contribution and arises primarily from the first (integral) term in (26). The rest of the bracketed expression is the  $T = 0$  quantum contribution from the fermionic degrees of freedom, and saturates at a constant value for large  $|y|$ . The remaining terms give the thermal contribution.

We want to use the above results to calculate the activation rate between the metastable and the true vacua. Our procedure will be as follows. We have an *exact* solution to the full, quantum equations of motion. To calculate the activation rate we can use the path integral formalism[19]; what we do is to saturate the path integral with the bubble configuration found above and evaluate the rate semiclassically. This is just the standard procedure that is commonly used. Thus, when we say we are calculating the “exact” activation rate, we mean that we are using the exact solution to the full equations of motion to perform the semiclassical calculation of the rate. In the large  $N$  approximation, our calculation would become exact in *all* senses of the word.

In the large  $N$  limit the gaussian fluctuations around the saddle point configuration yield a contribution of order  $(1/N)$  and to leading order the prefactor is 1. However the free energy  $F = N(F/N)$ , with  $F/N$  given by equation (27), and the rate formally vanishes in this limit.

For finite  $N$  we should take into account the corrections from the gaussian fluctuations around the saddle point configuration, that is the prefactor, this is an extremely difficult task in this case.

Therefore, we only concentrate on the exponential since it gives the leading behavior and in this case it contains the *quantum corrections* associated with the fermionic loops,



in particular in the case under consideration, the contribution to the exponential is *solely* arising from quantum corrections, since at tree level the auxiliary field has no dynamics.

Having clarified the nature of the approximations involved, we now set  $N = 1$ .

Given  $m$  and  $T$ , then, we can plot  $F$  as a function of  $y$  (Fig. 3), and the maximum is  $F_c^C$ . The superscript “C” indicates that this is the “Correct” method of calculating the critical bubble free energy. Up to a prefactor, the (semiclassical) activation rate is then  $\Gamma^C(T) = \exp(-F_c^C/T)$ . For  $m = 0.02$ ,  $\Gamma^C(T)$  is plotted as a solid curve in Figs. 5–8.

### 3 Some Approximation Schemes

Now we turn to the main point of this work, which is to compare the *exact* critical free energy in the GN model to that obtained by means of various approximations.

There are a variety of ways to approximate the free energy that enters into the activation rate. The class of schemes we consider involve approximating the kinetic term in various ways (note that the theory written in terms of the auxiliary field  $\Delta$  has no canonical kinetic term at tree level) as well as approximating the potential term. Some of these schemes will have counterparts in the  $3 + 1$  dimensional calculations of activation rates in scalar fields, while others are more specific to the Gross-Neveu model.

#### 3.1 The Landau-Ginzburg Approximation

The BCS theory of superconductivity contains a four-fermi interaction which controls the formation of Cooper pairs. A complex auxiliary field  $\phi$  can be introduced to rewrite this four fermi interaction as a Yukawa type coupling. This field then serves as an order parameter for the superconducting state. Its dynamics can be determined by integrating out the fermions and constructing the effective action for  $\phi$ . To understand the nature of the phase transition in this case, it is useful to perform a derivative expansion of the effective action near the critical temperature. This is the Landau-Ginzburg expansion[20]. We can perform the same procedure for the Gross-Neveu model.

The Landau-Ginzburg effective free energy is obtained as a consistent expansion in small order parameter ( $M$ ) and small gradients, and is valid near the critical temperature and for small explicit symmetry breaking fields (small  $m$ ). In this approximation (method “L”) the effective free energy density is written up to terms of order  $(\partial M(x)/\partial x)^2$  in the derivative expansion and up to order  $M^4(x)$  in the non-derivative (potential) terms. The calculation of the lowest gradient term is obtained via a Feynman diagram expansion to one loop using the imaginary time formulation of finite temperature field theory. It is carried out by writing  $M(x) = M + v(x)$  with  $M$  the *homogeneous* configuration, and  $v(x)$  (the small departure from

the homogeneous configuration) taken to be a perturbation. Due to the Yukawa coupling of  $M(x)$  to the fermions,  $M$  will be the mass of the fermions in the loop.

The coefficient of the gradient term is the bracketed expression in:

$$\frac{i}{2} \text{---} \bigcirc \text{---} = p^2 v(p) v(-p) \left[ \frac{1}{24\pi M^2} - \frac{1}{12\pi MT} I''' \left( \frac{M}{T} \right) \right] \quad (28)$$

where  $I(y)$  was defined in eq. (18). The diagram shows a fermion loop attached (with coupling  $v$ ) to two (truncated) scalar legs carrying spatial momentum  $p$ . The field  $v(x)$  is taken to be independent of the Matsubara frequencies, as well as slowly varying in space, in keeping with the philosophy of the derivative expansion. In the  $T \rightarrow 0$  limit the bracketed expression is  $1/(24\pi M^2)$ , while for  $T \gg M$  it is [using the expansion of eq. (19)]  $7\zeta(3)/(32\pi^3 T^2)$ . We have verified this calculation by means of Chan's method of obtaining the derivative expansion[21].

Using the quartic approximation (for  $T \gg M$ ) to the finite  $T$  effective potential of eq. (17) (see Fig. 4) yields the Landau-Ginzburg free energy density (per flavor):

$$\mathcal{F}^{\text{LG}} = \frac{7\zeta(3)}{32\pi^3 T^2} (\partial_x M)^2 - M m + \frac{M^2}{2\pi} [\ln(\pi T) - \gamma] + \frac{7\zeta(3)}{32\pi^3} \frac{M^4}{T^2} \quad (29)$$

This free energy density can be extremized with respect to  $M(x)$ , and it is found that the extremum inhomogeneous configuration is a bubble solution[22] which is of the same form as the true extremal bubble, eq. (21), with  $k_0$  fulfilling exactly the *same* integrability condition as in eq. (22). However, in this case,  $M_-$  is the local minimum of the Landau-Ginzburg potential, and for this extremal bubble,

$$k_0^2 = \frac{3M_-^2}{2} + \frac{4\pi^2 T^2}{7\zeta(3)} \ln(\pi T e^{-\gamma}) \quad (30)$$

With  $t \equiv k_0/|M_-|$ , the total free energy of this inhomogeneous configuration in the Landau-Ginzburg approximation is

$$F_c^L = \frac{7\zeta(3)}{4\pi^3 T^2} k_0^3 \left[ \frac{-4}{3} + \frac{2}{t^2} + \frac{1-t^2}{t^3} \ln \left( \frac{1-t}{1+t} \right) \right] \quad (31)$$

The exponential part of the activation rate,  $\Gamma^L(T) = \exp(-F_c^L/T)$ , is plotted as a dashed curve in Fig. 5, along with the correct result  $\Gamma^C(T)$ ; from this graph we see that method “L” overestimates the rate up until the critical temperature where they both become equal to unity (the critical temperatures are slightly different). This feature will recur in all the approximation schemes we use here, except for the last (zero  $T$  bubble).

### 3.2 Landau-Ginzburg With $T = 0$ Gradients

In method “G”, the same Landau-Ginzburg potential is used, but only the  $T = 0$  gradient term is taken, *i.e.* the coefficient in front of the derivative term is  $1/(24\pi M_-^2)$ . The critical

bubble free energy is then given by

$$F_c^G = \frac{F_c^L}{R}, \quad R \equiv \sqrt{24\pi M_-^2} \sqrt{\frac{7\zeta(3)}{32\pi^3 T^2}} \quad (32)$$

where  $F_c^L$  was given in eq. (31).  $\Gamma^G(T) = \exp(-F_c^G/T)$  is plotted as a dashed curve in Fig. 6.

This method is closer in spirit to the one used in the standard calculations[19] of finite temperature activation rates for scalar field theories with canonical kinetic terms. In these calculations, the canonical kinetic term is combined with the finite- $T$  effective potential to give the free energy relevant to the activation rate.

### 3.3 The Effective Potential Approximation

In the effective potential approximation (method “P”), we define

$$F^{\text{pot}} = \int dx [V_{\text{eff}}(M(x)) - V_{\text{eff}}(M_-)] \quad (33)$$

where  $V_{\text{eff}}$  was defined in eq. (17). Among configurations of the form eq. (21) [and satisfying the integrability condition eq. (22)], parameterized by the half-width  $y$ , we choose  $y$  to extremize  $F^{\text{pot}}$ , and the resulting  $F^{\text{pot}}$  is our approximation to the critical free energy  $F_c^P$ .  $\Gamma^P(T) = \exp(-F_c^P/T)$  is plotted as a dashed curve in Fig. 7.

Since *classically* there is no kinetic term in our Lagrangian, eq. (2), this method is tantamount to *ignoring derivative corrections* (both quantum and thermal). In real-world calculations, such as that of the free energy of a critical bubble or the mass of a sphaleron, derivative corrections are often ignored [23]; the finite- $T$  effective potential is combined with the classical (canonical) kinetic term, and the resulting approximate action is extremized.

For example, the sphaleron mass at  $T = 0$  is known to be [24]

$$M_{\text{SP}} = \frac{4\pi v B}{g}, \quad (B = 1.5 - 2.7) \quad (34)$$

where  $v$  is the minimum of the Higgs potential. The sphaleron mass at finite  $T$  is then approximated by the same formula but with  $v \rightarrow v(T)$ , the minimum of the Higgs effective potential [and also  $g \rightarrow g(T)$ ]. Derivative corrections to the action have been ignored.

### 3.4 The Zero- $T$ Bubble

In the zero- $T$  approximation (method “Z”), the approximation scheme is as follows. We start by finding the  $T = 0$  critical bubble, a configuration of the form eq. (21) and eq. (22), with  $M_-$  the minimum of *zero temperature* effective potential,  $V_{\text{eff}}(T=0)$ , choosing  $y$  to extremize the  $T = 0$  free energy. Then we plug this value of  $y$  into the *finite- $T$*  formula for the free energy, eq. (27).  $\Gamma^Z(T) = \exp(-F_c^Z/T)$  is plotted as a dashed curve in Fig. 8.

This is analogous to the method used for critical bubbles in [23]. There the bubble configuration used was the extremum of the classical,  $T = 0$  action. The (1-loop) finite- $T$  free energy of this bubble was then calculated (exactly, including “derivative corrections”) by numerically evaluating the determinant factor.

The purpose of ref. [23] was to measure “derivative corrections” by comparing the Zero- $T$  calculation (which includes derivative corrections) to the effective potential calculation (which does not). This effort was hampered by the fact that the Zero- $T$  calculation is itself an approximation (only good at lower temperatures). In the Gross-Neveu model of this paper, we can compare both methods to the true result.

## 4 Finite Fermion Number

If sphaleron configurations are relevant in baryon number violating processes, an important question to pose is how the presence of a finite baryon number modifies the field profile and the free energy barrier of the sphaleron configuration. Within the model under consideration we can provide some partial answers to these questions. In this model we identify baryon number with fermion number. In order to consider a finite baryon number *density* at zero temperature we would have to allow for the case in which the  $N$  positive energy fermion bound states are occupied, and the rest of the baryons to be in the positive energy continuum up to a Fermi energy (or chemical potential). Because the phase shifts of the continuum states depend on the bubble “collective coordinate”  $y$ , to obtain the bubble profile for arbitrary  $y$ , the Fermi energy will have to be adjusted such as to provide the constant baryon density (a constraint on the system).

At finite temperature we would have to introduce a chemical potential and work in the grand canonical ensemble, finally fixing the chemical potential (as a function of temperature and bubble size) to give the fixed baryon number density (on average). Both situations are extremely hard to implement and at the present time lie beyond our capabilities.

We will content ourselves with considering the somewhat more restricted scenario in which we have a *fixed baryon number* ( $B$ ),  $0 < B \leq N$  and the case of zero temperature. The reason that this case is somewhat simpler is that we can accommodate the  $B$  baryons in the available  $N$  positive energy bound states. This corresponds to the ground state configuration with a finite (positive) baryon number  $B \leq N$  (for a negative baryon number we would have to deplete  $B$  *negative* energy bound states).

Following the steps leading to (27) at  $T = 0$  we find that the free energy becomes

$$\frac{F^B}{N} = \frac{F^0}{N} + \frac{B}{N}\omega_0 \quad (35)$$

with  $F^0$  given by equation (27) with  $T = 0$ . It is convenient to parametrize

$$\begin{aligned}
k_0 &= |M_-| \sin(\theta) \\
\omega_0 &= |M_-| \cos(\theta) \\
y(\theta) &= \frac{1}{4 \sin(\theta)} \ln \left[ \frac{1 + \sin(\theta)}{1 - \sin(\theta)} \right] \\
0 &\leq \theta \leq \pi/2
\end{aligned} \tag{36}$$

Since  $y(\theta)$  is a monotonically increasing function of  $\theta$  it proves more convenient to locate the size of the critical bubble by extremizing the free energy with respect to  $\theta$ . The extremum condition leads to

$$-\frac{m}{|M_-|} \tan(\theta) + \frac{\theta}{\pi} = \frac{B}{2N} \tag{37}$$

As we have analyzed in section two, the metastable minimum is available only for  $\pi m/|M_-| < 1$ . Thus we find that for  $B \neq 0$  there are two *non-trivial* extrema of the energy functional. Clearly one corresponds to a minimum and the other to the maximum, i.e. the critical bubble. The free energy barrier between the minimum and the maximum becomes smaller as  $B$  is increased, finally disappearing at a maximum baryon number given by  $B_{max}$  where  $B_{max}$  is found using  $\theta_{max} = \sin^{-1} \left( \sqrt{1 - \pi \frac{m}{|M_-|}} \right)$  in eq. (37).

For  $B > B_{max}$  the barrier disappears altogether and there is no longer a bubble solution. This is indeed a remarkable result if it persists in three dimensions. The physics of this phenomenon is clear. By filling up the allowed positive energy bound states the Pauli pressure (a consequence of the Pauli exclusion principle) increases. For the minimum which appears at a *smaller* bubble radius this pressure is larger than that for the maximum, which appears for a larger bubble radius. Although extrapolation to three dimensions is not warranted, we would expect fermionic bound states in the lowest ( $J = 1/2$ ) partial wave, because in this partial wave the problem is essentially one-dimensional (save for the fact that the wave function must satisfy proper boundary conditions at the origin). If the effect of these fermionic bound states localized at the wall of the bubble is consistent with the behavior just found in this 1 + 1 dimensional model, it would imply that the current bounds on sphaleron transitions may be a gross *underestimate* for the rate. Clearly we cannot conclude that this happens in the more realistic three dimensional scenario, but we believe that this observation may be worthy of consideration there as previous estimates did not take into account the fermionic back-reaction onto the sphaleron configuration and their effect on the activation barriers.

## 5 Results and Conclusions

The amazing thing about the GN model is that one can calculate the *exact* critical bubble configuration of the theory and hence we can deduce the true (modulo our statements about the semiclassical evaluation of the relevant path integral) value of the activation rate (or at least its exponential part, which typically is the most important part of the rate).

$\Gamma(T) = e^{-F_c/T}$  calculated by our several methods (one exact and four approximations) are plotted in Figs. 5–8 (for  $m = 0.02$  and  $N = 1$ ). The bubbles  $M(x)$  (for  $m = 0.02$ ,  $N = 1$ , and  $T = 0.35$ ) used in these methods are plotted in Fig. 9.

We see that the Landau-Ginzburg method (“L”) and the potential method (“P”) converge nicely to the correct result (“C”) at high temperatures. They both correctly predict  $\Gamma(T_c) = 1$ , though their respective critical temperatures vary slightly from the correct  $T_c$ ; we would only expect exact agreement if the phase transition were second order (the limit  $m \rightarrow 0$ ). The zero-T method (“Z”) is a poor approximation at higher temperatures, but is better at lower  $T$ ’s. Curiously, all the approximation schemes tend to overestimate the rate.

Finally, we have to address the question of what this means for realistic field theories in  $3+1$  dimensions. Since the GN model was so special in that we could find the exact bubbles, etc., one might be tempted to think that our results should only hold for this model. While we have no evidence that this is not the case, it should be recalled that the GN model serves as a very good testing ground for issues such as asymptotic freedom, which does in fact occur in  $3+1$  field theories. It is also the inspiration for Nambu-Jona-Lasinio low energy effective models for strong interactions. Thus, our results may have a wider range of applicability to theories in higher dimensions. In particular, if the various sphaleron configurations in higher dimensional theories can sustain fermionic bound states, then we expect that our discussion of the activation rate in the presence of finite fermion number should apply. This would be of great importance since the reduction of the barrier would have significant consequences for the activation rate.

At any rate, what our results *do* show is that the standard methods of calculating the activation rate need not be all that close to the exact value; if nothing else, our calculation can serve as a warning sign to those who might believe their approximations overly much.

## Acknowledgements

DB and DSL were partially supported by NSF Grant # PHY-9302534. DSL was also supported by a Mellon Fellowship. DEB and RH were partially supported by the U.S. Dept. of Energy under Contract DE-FG02-91-ER40682.

## References

- [1] For a comprehensive review see: P. Hanggi, P. Talkner and M. Borkovec, Rev. of Mod. Phys. 62, 251 (1990).
- [2] D.A. Kirzhnits and A.D. Linde, Phys. Lett. 42B, 471, (1972).
- [3] For a good review, see “Anomalous Fermion Number Non-Conservation” by M.E. Shaposhnikov, CERN preprint CERN-TH.6304/91 (1992).
- [4] S. Coleman, Phys. Rev. D15:2929 (1977), 16:1248(E) (1977);  
C.G. Callan and S. Coleman, Phys. Rev. D16:1762 (1977);  
S. Coleman, “The Uses of Instantons”, *Proc. 1977 Int. School of Subnuclear Physics, Ettore Majorana*, ed. A. Zichichi (Plenum, New York, 1979); reprinted in *Aspects of Symmetry* (Cambridge University Press, 1985).
- [5] J.W. Cahn and J.E. Hilliard, J. Chem. Phys. 31:688 (1959);  
J.S. Langer, Ann. Phys. 41:108 (1967); *ibid.* 54:258 (1969);  
M.B. Voloshin, I.Y. Kobzarev and L.B. Okun, Yad. Fiz. 20:1229 (1974) [Sov. J. Nucl. Phys. 20:644 (1975)];  
P.H. Frampton, Phys. Rev. D15:2922 (1977);  
A.D. Linde, Phys. Lett. 70B:306 (1977); *ibid.* 100B:37 (1981); Nucl. Phys. B216:421 (1983); *ibid.* B223:544 (1983)(E);  
O.J.P. Éboli and G.C. Marques, Rev. Bras. Fís. 16:147 (1986).
- [6] M. Gleiser, G.C. Marques and R.O. Ramos, Phys. Rev. D48:1571 (1993).
- [7] D. J. Gross and A. Neveu, Phys. Rev. D10, 2443 (1974).
- [8] S. Coleman “ $1/N$ ”, in *Aspects of Symmetry* (Cambridge University Press, 1985).
- [9] L. Dolan and R. Jackiw, Phys. Rev. D9, 3320 (1974).
- [10] R. F. Dashen, B. Hasslacher and A. Neveu, Phys. Rev. D12, 2443 (1975).
- [11] D. K. Campbell and Y-T. Liao, Phys. Rev. D14, 2093, (1976).
- [12] D. K. Campbell and A. R. Bishop, Nucl. Phys. B200[FS4], 297 (1982); Phys. Rev. B24, 4859 (1981).
- [13] K. Fesser, A. R. Bishop and D. K. Campbell, Phys. Rev. B27, 4804 (1983); Mol. Cryst. Liq. Cryst. 77, 253 (1981).
- [14] S. A. Brazovskii and N. Kirova, Sov. Phys. Lett. (JETP) 33, 4 (1981).

- [15] D. Boyanovsky, C. A. de Carvalho and E. Fraga, Phys. Rev. B50, 2889 (1994)
- [16] R. Jackiw and C. Rebbi, Phys. Rev. D13, 3398 (1976).
- [17] R. Jackiw and J. R. Schrieffer, Nucl. Phys. B190, 253 (1981).
- [18] N. S. Manton and T. M. Samols, Phys. Lett. B207, 179 (1988).
- [19] A. D. Linde, Phys. Lett. 70B, 306 (1977); Phys. Lett. 100B, 37 (1981); Nucl. Phys. B216, 421 (1983) and in “Particle Physics and Inflationary Cosmology” (Harwood Academic, 1990)
- [20] B. Sakita, “Quantum Theory of Many-Variable Systems and Fields” (World Scientific, 1985)
- [21] L.-H. Chan, Phys. Rev. Lett. 54:1222 (1985); Phys. Rev. Lett. 56:404(E) (1986).
- [22] C. A. de Carvalho, C. A. Bonato and G. B. Costamilan, J. Phys. A: Math. and Gen. 22, L1153-L1157 (1989);  
D. Boyanovsky and C. A. de Carvalho, Phys. Rev. D48, 5850 (1993).
- [23] D. Brahm and C.L.Y. Lee, Phys. Rev. D49:4094 (1994).
- [24] F.R. Klinkhamer and N.S. Manton, Phys. Rev. D30:2212 (1984).



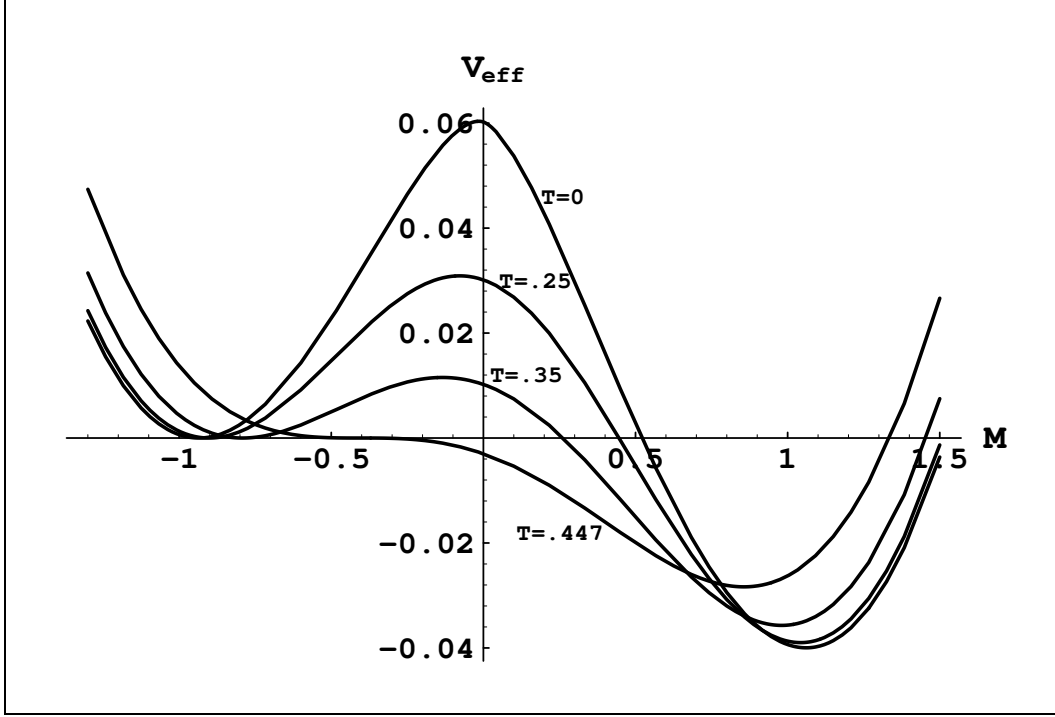


Fig. 1:  $V_{\text{eff}}(M)$  for  $m = .02$  and  $T = \{0, .25, .35, .447\}$ .

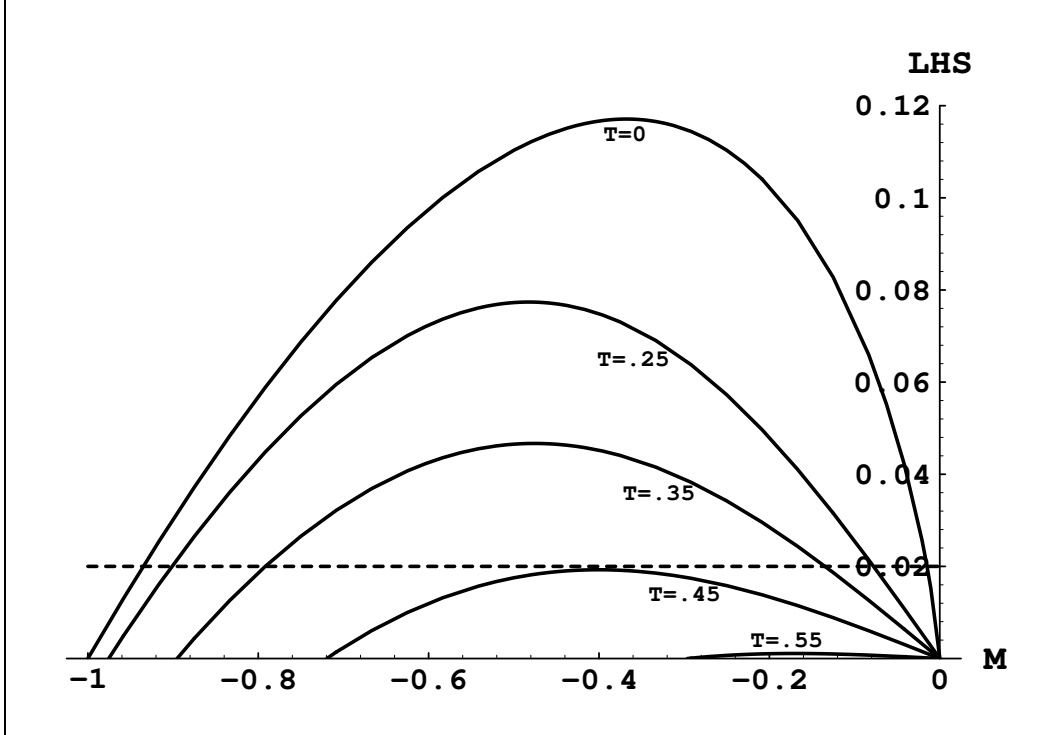


Fig. 2: Left-hand side (LHS) of the gap equation at  $T = \{0, .25, .35, .45, .55\}$ . Dashed line is  $m/\lambda_R = .02$ , for which the critical temperature is  $T_c = .447$ .

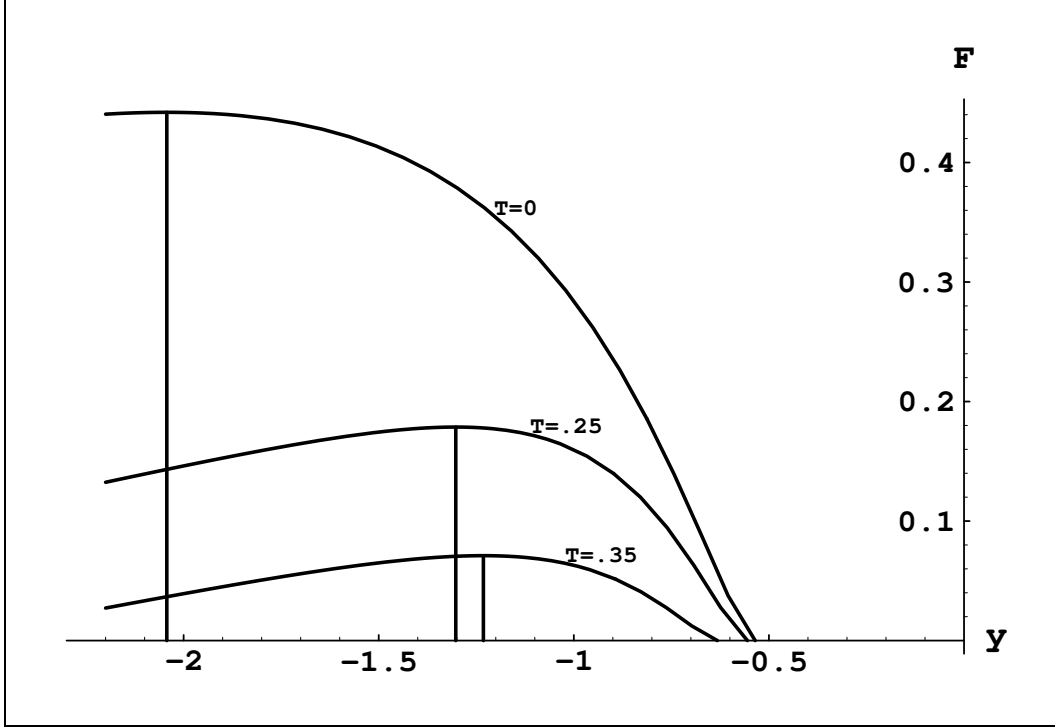


Fig. 3: Bubble free energy  $F(y)$  as a function of the half-width  $y$ , for  $m = .02$  and  $T = \{0, .25, .35\}$ . The maximum (for a given  $T$ ) is the critical free energy  $F_c$ .

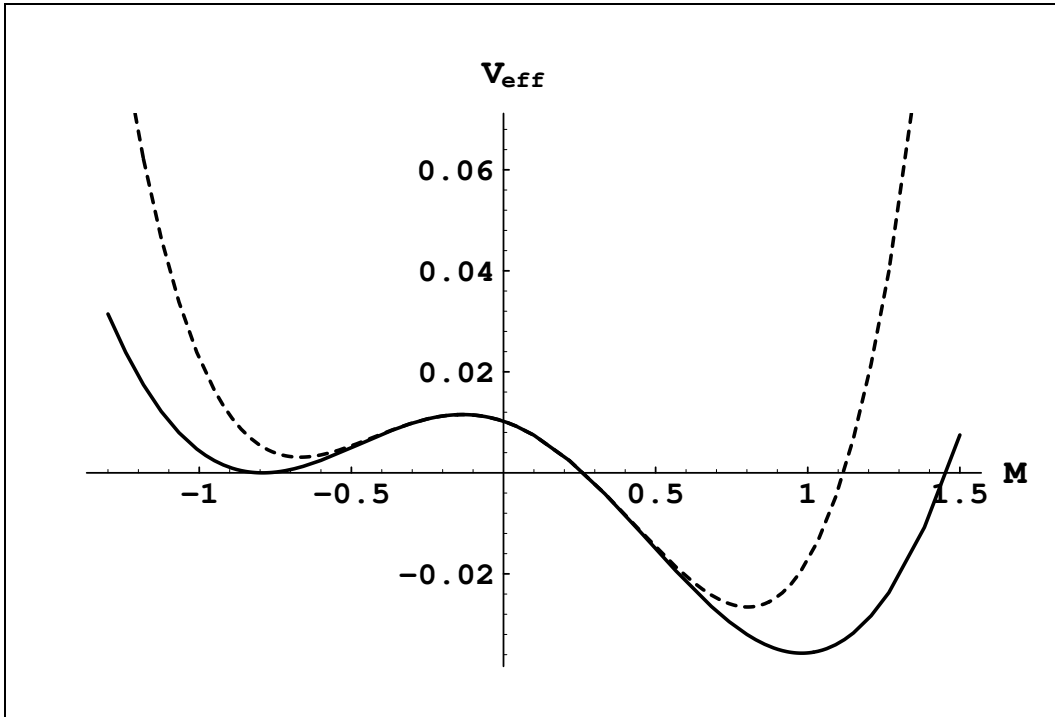


Fig. 4: True  $V_{\text{eff}}(M)$  (solid) and the Landau-Ginzburg approximation (dashed), for  $m = .02$  and  $T = .35$ .

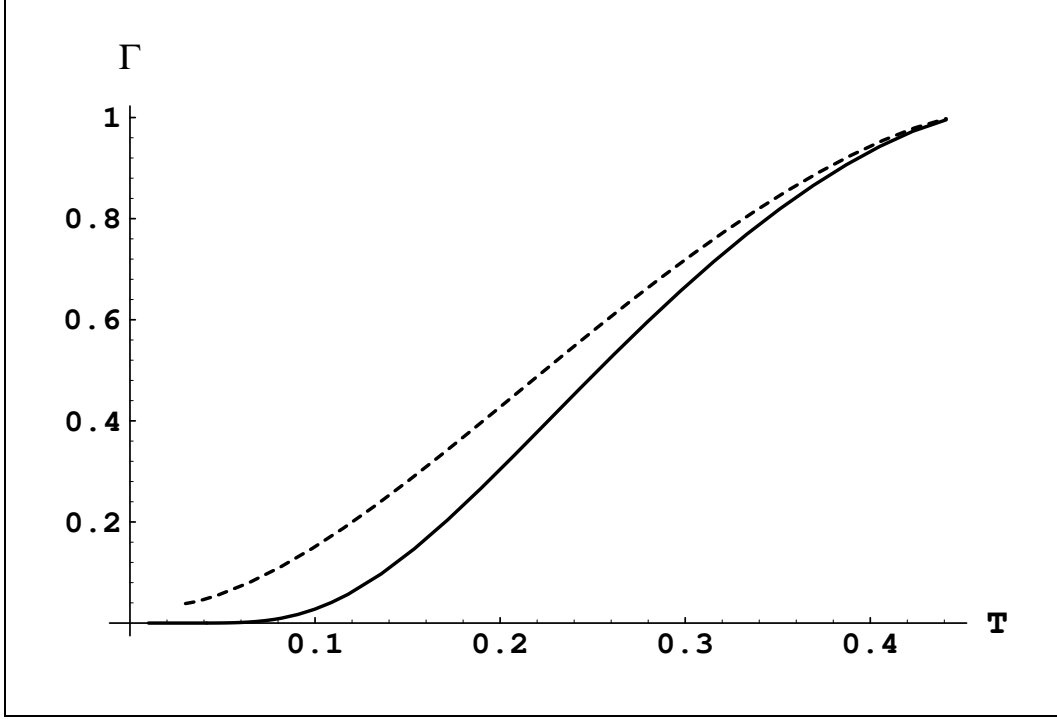


Fig. 5:  $\Gamma(T) = e^{-F_c(T)/T}$  for  $m = .02$ : solid = C (Correct),  
dashed = L (Landau-Ginzburg).

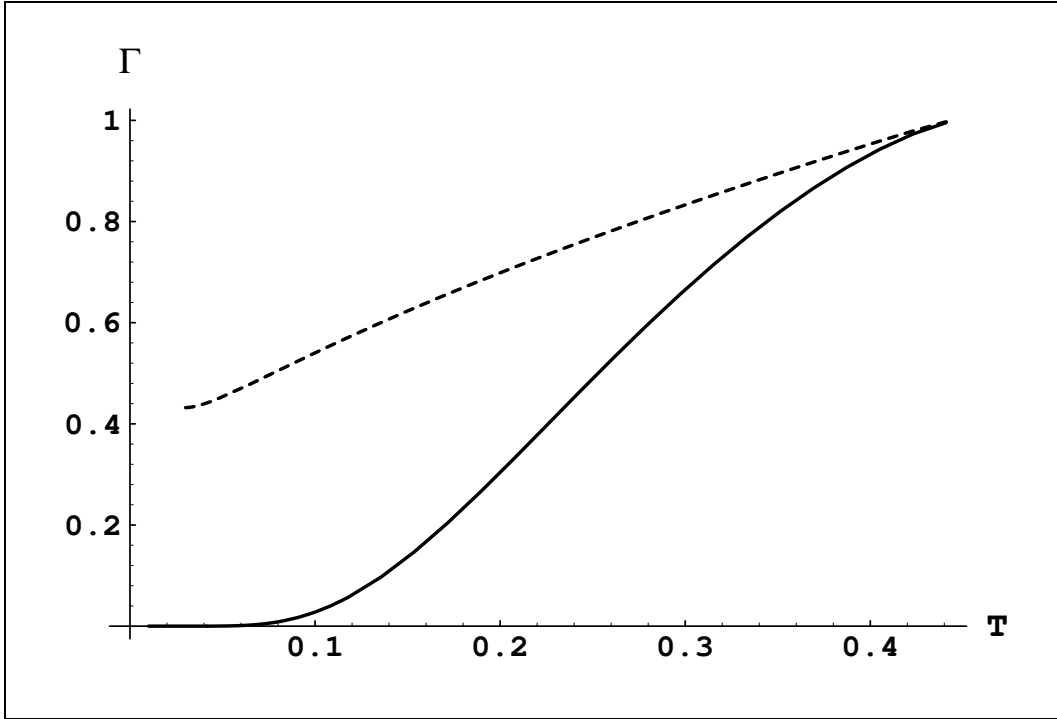


Fig. 6:  $\Gamma(T) = e^{-F_c(T)/T}$  for  $m = .02$ : solid = C (Correct),  
dashed = G (Landau-Ginzburg With  $T = 0$  Gradients).

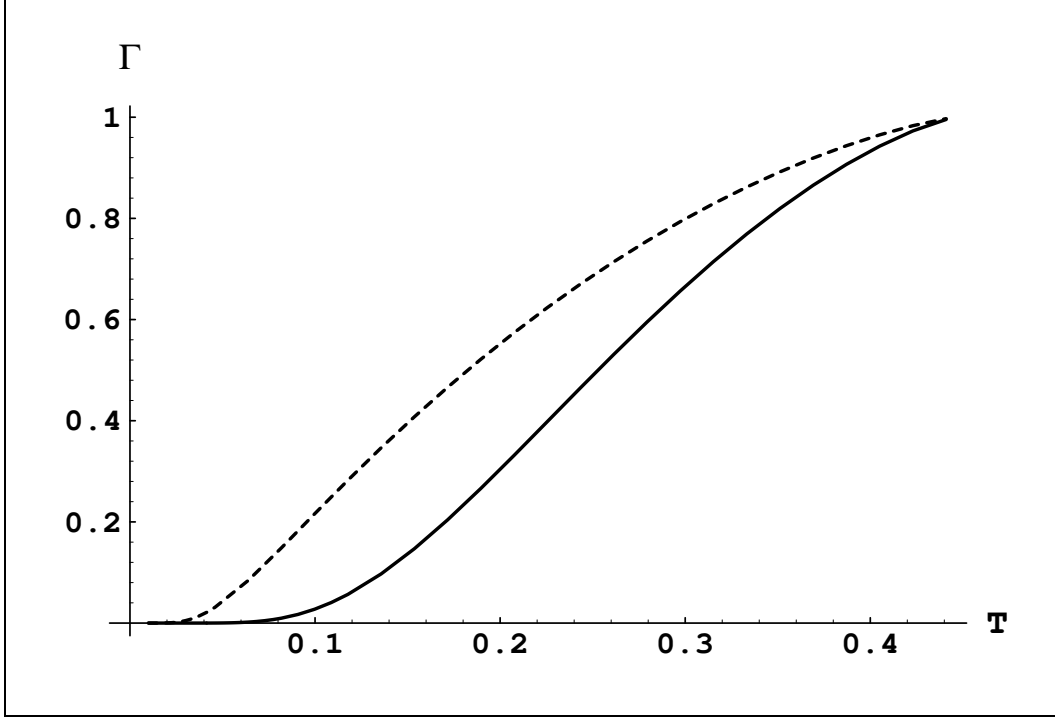


Fig. 7:  $\Gamma(T) = e^{-F_c(T)/T}$  for  $m = .02$ : solid = C (Correct), dashed = P (Potential).

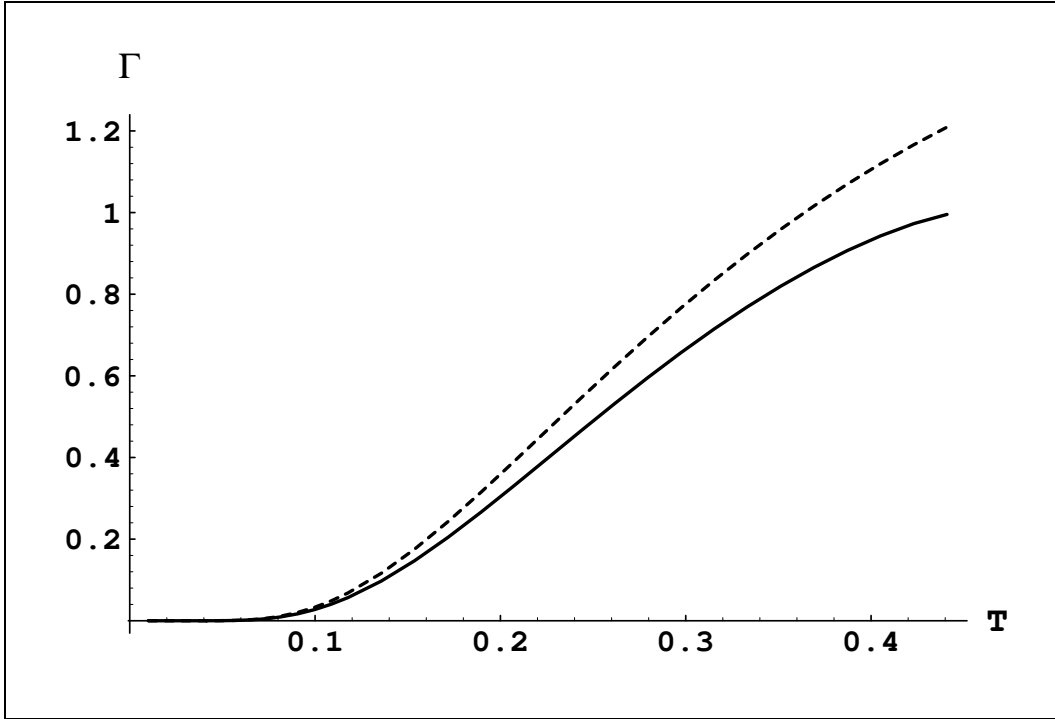


Fig. 8:  $\Gamma(T) = e^{-F_c(T)/T}$  for  $m = .02$ : solid = C (Correct), dashed = Z ( $T = 0$  bubble).

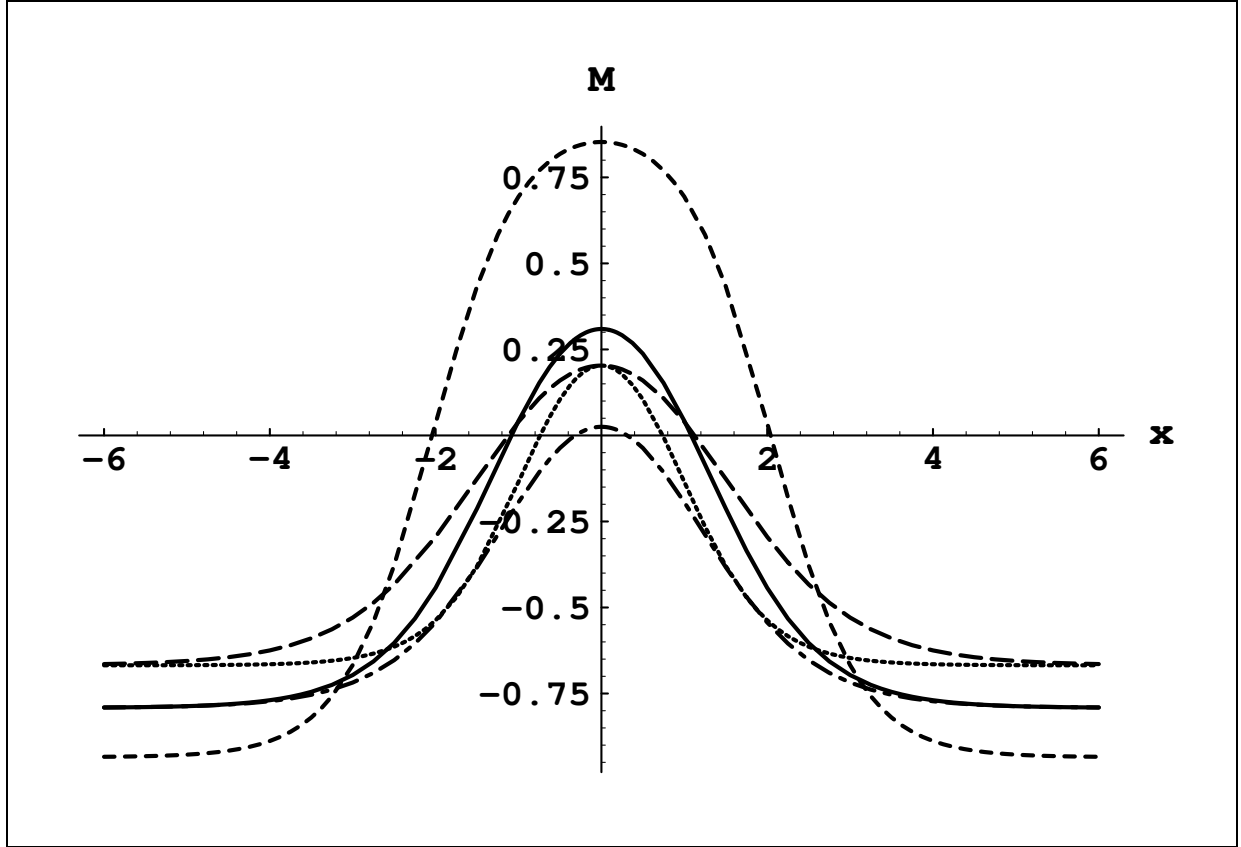


Fig. 9: Critical bubbles  $M(x)$  for  $m = .02$  and  $T = .35$ , five methods:  
solid = C (Correct), long-dash = L (Landau-Ginzburg),  
dots = G (Landau-Ginzburg With  $T = 0$  Gradients),  
dot-dash = P (Potential), short-dash = Z ( $T = 0$  bubble).